Large Second-Harmonic Response and Giant Birefringence of $CeF_2(SO_4)$ Induced by Highly Polarizable Polyhedra

Chao Wu,[†,¶] Tianhui Wu,[†,¶] Xingxing Jiang,[‡,¶] Zujian Wang,[§,¶] Hongyuan Sha,[§] Lin Lin,[†] Zheshuai Lin,[‡] Zhipeng Huang,[†] Xifa Long,[§] Mark G. Humphrey,[ξ] and Chi Zhang[†,*]

[†] China-Australia Joint Research Center for Functional Molecular Materials, School of Chemical Science and Engineering, Tongji University, Shanghai 200092, China

[‡] Technical Institute of Physics and Chemistry, Chinese Academy of Sciences, Beijing 100190, China

[§] Key Laboratory of Optoelectronic Materials Chemistry and Physics, State Key Laboratory of Structure Chemistry, Fujian Institute of Research on the Structure of Matter, Chinese Academy of Sciences, Fuzhou, Fujian 350002, China

[ξ] Research School of Chemistry, Australian National University, Canberra, ACT 2601, Australia

Supporting Information Placeholder

ABSTRACT: Second-harmonic generation (SHG) response and birefringence are two critically important properties of nonlinear optical (NLO) materials. However, the simultaneous optimization of these two key properties remains a major challenge because of their contrasting microstructure requirements. Herein, we report the first tetravalent rare-earth metal fluorinated sulfate, $CeF_2(SO_4)$. Its structure features novel net-like layers constructed by highly-distorted $[CeO_4F_4]$ polyhedra, which are further interconnected by $[SO_4]$ tetrahedra to form a three-dimensional structure. $CeF_2(SO_4)$ exhibits the strongest SHG effect (8 times that of KH_2PO_4) and the largest birefringence for sulfate-based NLO materials, the latter exceeding the birefringent limit for oxides. Theoretical calculations and crystal structure analysis reveal that the unusually large SHG response and giant birefringence can be attributed to the introduction of the highly polarizable fluorinated $[CeO_4F_4]$ polyhedra as well as the favorable alignment of $[CeO_4F_4]$ polyhedra and $[SO_4]$ tetrahedra. This research affords a new paradigm for the designed synthesis of high-performance NLO materials.

Nonlinear optical (NLO) crystalline materials with second harmonic generation (SHG) properties play a crucial role in modern laser science and technology because their frequency conversion abilities can extend the output spectral ranges of laser sources.[1-6] In the past decades, a few NLO materials have been discovered and commercialized,[7] such as $KBe_2BO_3F_2$ (KBBF),[8] β-BaB_2O_4 (BBO),[9] LiB_3O_5 (LBO),[10] and $AgGaS_2$ (AGS).[11] The desirable characteristics for excellent NLO materials are large SHG response and sufficient birefringence to achieve phase matching in a specific transparency window.[12-16] However, it is exceptionally challenging to simultaneously maximize these two optical parameters because they impose different requirements on the microstructure. For example, the NLO crystal SrB_4O_7[17,18] exhibits a strong SHG response originating from the aligned arrangement of tetrahedral $[BO_4]$ units, but it suffers from a small birefringence caused by the nearly isotropic configuration of the corner-sharing $[BO_4]$ groups. Efficient routes to new NLO materials with large SHG response and birefringence are consequently of enormous current academic and commercial interest.[3-6,12-16]

Inorganic oxides based on tetrahedral groups,[19] including phosphates,[20-24] silicates,[25] and sulfates,[26-28] are promising candidates for NLO materials because of advantages in their environmentally friendly chemical compositions, wide transmittance ranges, and ease of crystal growth. Notable examples include commercially available KH_2PO_4 (KDP)[20] and $KTiOPO_4$ (KTP)[7] as well as the recently developed $LiCs_2PO_4$,[22] $Ba_2NaClP_2O_7$,[23] $NH_4NaLi_2(SO_4)_2$,[26] and Li_2BaSiO_4.[25] However, due to the small microscopic second-order polarizability and the weak optical anisotropy of the tetrahedral groups,[29] the majority of these crystalline materials display weak SHG signals and/or small birefringence that seriously hinder their practical applications. Thus far, the design strategies for enhancing the SHG response and birefringence of tetrahedral group-based oxides have mainly focused on the introduction of cations susceptible to second-order Jahn−Teller (SOJT) distortions [lone-pair cations (e.g., I^+, Pb^{2+}, Sn^{2+}, Sb^{3+})[30-33] and octahedrally coordinated d^0 transition metals (d^0 TMs, e.g., Ti^{4+}, Nb^{5+}, W^{6+})[34,35]]. In comparison, the incorporation of non-SOJT structural units into tetrahedral group-based oxides has been largely ignored as a means to create new NLO materials with both strong SHG response and large birefringence.

In principle, optical properties are related to the electronic structures of the conduction band (CB) minimum and valence band (VB) maximum, which are influenced by the constituent elements, chemical bond types, and molecular stacking configurations. Our previous research has demonstrated that non-SOJT structural units offer tremendous possibilities for tuning linear and nonlinear optical properties.[36] In the present study, we propose a strategy of increasing structural distortion by the introduction of non-SOJT fluorinated rare-earth (RE) metal-centered polyhedra, as a means to enhance the NLO response and the birefringence. Unlike SOJT cations, rare-earth cations (particularly those with localized 4f electrons[37]) can induce significant differences in the band structures and thereby potentially improve the linear and nonlinear optical properties. Polarizable polyhedra[38] can be easily formed through the partial substitution of O^{2-} in RE-centered polyhedra with the more electronegative F^-, due to the increased ionicity of the RE-F bonds. Tetrahedral anionic groups, which are controlled by polarizable metal-centered polyhedra, may exhibit enhanced optical anisotropy and polarizability when they are aligned uniformly;[23] this favors the maximization of SHG response and birefringence simultaneously. Following this strategy to increase the structural distortion, the first tetravalent rare-earth

fluorinated sulfate $CeF_2(SO_4)$ has been successfully constructed, with its 3D structure built from highly polarizable $[CeO_4F_4]$ polyhedra and $[SO_4]$ tetrahedra. Owing to its simple chemical composition, millimeter-size crystals can be easily obtained via facile hydrothermal methods. $CeF_2(SO_4)$ exhibits the strongest SHG response (8 × KDP) among the sulfate-based NLO materials, and its large birefringence (0.361 at 546 nm) breaks through the birefringent limit for oxides. Herein, we report its synthesis, crystal structure, linear and nonlinear optical properties, as well as computational studies to rationalize its excellent performance.

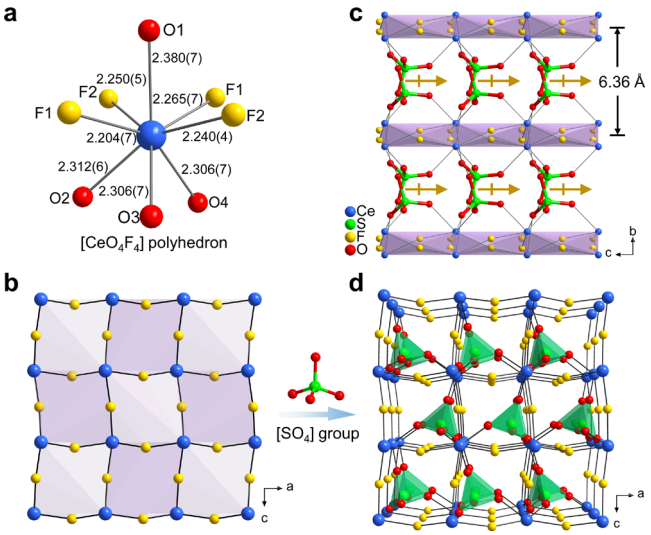

Figure 1. (a) Coordination environment of the Ce atoms in $CeF_2(SO_4)$. (b) View of the 2D $[CeF_2]_\infty$ framework along the *b* axis. Oxygen atoms have been omitted for clarity. (c) View of the $CeF_2(SO_4)$ structure along the *a* axis. Khaki arrows indicate the dipole moment direction of adjacent $[SO_4]$ groups. (d) Structure of $CeF_2(SO_4)$ viewed along the *b* axis.

Single crystals of $CeF_2(SO_4)$ with dimensions up to millimeters on a side were synthesized in a hydrothermal reaction of a mixture of CeO_2, H_2SO_4, 40% HF, and H_2O at 230 °C for 3 days. A photograph of the transparent yellow blocks is shown in Figure 2a (the largest is 2.0 × 1.2 × 0.4 mm^3). The yellow crystals are stable in air for six months without weight loss or change in appearance. Powder X-ray diffraction (XRD) analysis confirmed the purity of the product (Figure S1). Energy dispersive spectroscopy analysis of crystalline $CeF_2(SO_4)$ verified the presence of Ce, S, O, and F elements, as shown in Figure S2. Thermogravimetric analysis (Figure S3) indicates that $CeF_2(SO_4)$ is thermally stable up to 405 °C and exhibits a two-step weight loss: the minor weight loss of 7.22% that occurs in the range 405−520 °C is due to the loss of F_2 (calculated value 6.93%), while in the second stage (550−830 °C) the weight loss of 28.29% is tentatively attributed to the release of O_2 and SO_2 (calculated value 27.2%). The final residuals at 900 °C were confirmed by the powder XRD study to be mainly CeO_2 and CeF_3 (Figure S4).

$CeF_2(SO_4)$ crystallizes in the non-centrosymmetric (NCS) and polar orthorhombic space group $Pca2_1$ (No. 29, Table S1). Within one asymmetric unit, there are one independent Ce, one S, four O, and two F atoms (Figure S5a). Each Ce atom is eightfold coordinated by four O atoms from four $[SO_4]$ groups and four fluoride atoms, forming a distorted $[CeO_4F_4]$ polyhedron with Ce-O distances ranging from 2.306(6) to 2.380(7) Å and Ce-F distances in the range 2.204(7) to 2.265(7) Å (Table S2). The fluorine atoms act as structure directing agents, significantly affecting the coordination environment of the Ce^{4+} cation, and leading to the formation of fluorinated tetravalent cerium-centered polyhedra with large local dipole moments (Figure 1a). Owing to the unique coordination environment and localized 4f electrons on the Ce^{4+} cation, the highly distorted $[CeO_4F_4]$ polyhedron is conducive to the generation of large optical anisotropy and hyperpolarizability. Contiguous $[CeO_4F_4]$ units are linked in a corner-sharing [F(1) and F(2)] mode, leading to distorted eight-membered squares in the $[CeF_2]_\infty$-layer-containing *ac* plane (Figures 1b and S5b), with the ordered in-plane arrangement of the $[CeO_4F_4]$ units playing an important role in further enhancing the birefringence and SHG response. The distance between adjacent $[CeF_2]_\infty$ layers is 6.36 Å (Figure 1c). Asymmetric $[SO_4]$ groups are located in the $[Ce_4F_4]$ eight-membered rings, serving as interlayer linkers connecting four Ce atoms (Figure S5c), and thereby forming the final three-dimensional structure (Figure 1d). The $[SO_4]$ tetrahedra are aligned roughly parallel to the *c* axis (Figure 1c), a spatial arrangement that additively enhances the optical anisotropy and allows $CeF_2(SO_4)$ to display birefringence. Bond valence sum calculations on Ce^{4+}, S^{6+}, O^{2-}, and F^- gave values of 3.87, 6.05, 1.90−2.02, and 1.02−1.05, respectively (Table S3).

The SHG intensities of crystalline powder samples under 1064 nm laser irradiation indicate that $CeF_2(SO_4)$ not only exhibits a large SHG effect (8 × KDP) within the 105−150 μm particle size range, but also realizes phase-matching at 1064 nm (Figures 2a and 2b). To the best of our knowledge, $CeF_2(SO_4)$ shows the largest SHG response among reported sulfate-based NLO materials (Table S4). The optical performance was also probed by first-principles calculations.[39] The non-zero independent SHG coefficients (d_{31}, d_{32}, and d_{33}), under the restriction of Kleinman symmetry, are as follows: $d_{31} = -6.316$ pm/V, $d_{32} = -7.356$ pm/V, and $d_{33} = -10.945$ pm/V (Table S6).[40,41] The calculated average SHG coefficient is larger than the experimental result, which can be attributed to the fact that the SHG calculations are based on an optimized single-crystal structure that may generate a larger SHG effect. The origin of the SHG effect was explored further via an SHG-weighted electron density analysis. It is clear that the SHG-weighted electron clouds of d_{33} are mainly located on the $[CeO_4F_4]$ and $[SO_4]$ units (Figures 2c and 2d). The nonbonding O-2p orbitals make a significant contribution to the SHG effect in the occupied states, while in the unoccupied states, the Ce-4f orbitals afford the primary contribution to the SHG response. These results indicate that under the perturbation of ambient optoelectronic fields, the SHG contribution of $[CeO_4F_4]$ units is significantly larger than that of the $[SO_4]$ units (Figure 2d). The specific SHG contributions from all units were calculated by a real-space

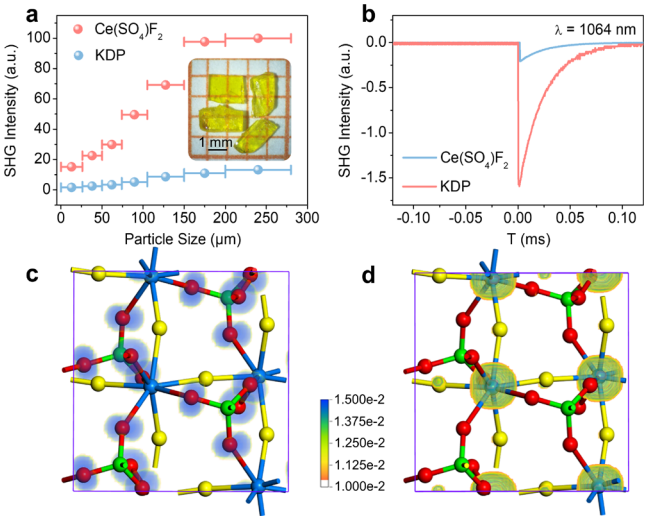

Figure 2. (a) Phase-matching curve of $CeF_2(SO_4)$ with 1064 nm laser radiation. KDP was used as a reference for the SHG measurement at 1064 nm. The inset shows a photograph of $CeF_2(SO_4)$ single crystals. (b) Oscilloscope traces of the SHG signals for powders of $CeF_2(SO_4)$, and KDP in the same particle size range

105−150 μm. SHG-weighted densities for (c) occupied and (d) unoccupied electronic states of $CeF_2(SO_4)$.
atom-cutting method. As shown in Table S6, the contributions to the largest SHG coefficient d_{33} are 9.846 pm/V for $[CeO_4F_4]$ (96.5% of d_{33}) and 0.358 pm/V for $[SO_4]$ (3.5% of d_{33}). It is evident that, in comparison to $[SO_4]$, the $[CeO_4F_4]$ units make the dominant contributions to the SHG coefficients in $CeF_2(SO_4)$, which is in good agreement with the SHG-weighted electron density analysis.

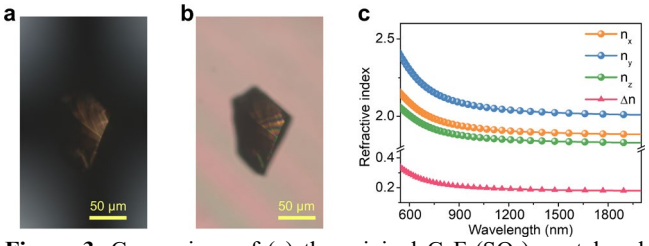

Figure 3. Comparison of (a) the original $CeF_2(SO_4)$ crystal and (b) the $CeF_2(SO_4)$ crystal achieving complete extinction. (c) Calculated frequency-dependent refractive indices of $CeF_2(SO_4)$.

The birefringence of a $CeF_2(SO_4)$ single crystal was measured on a ZEISS Axio A1 polarizing microscope (Figure 3a), demonstrating complete extinction (Figure 3b). The retardation value of the measured crystal was approximately 6.78 μm with a thickness of 18.8 μm (Figure S6), corresponding to a measured birefringence of 0.361 at the wavelength of 546 nm. The birefringence of $CeF_2(SO_4)$ is larger than those of the commercial birefringent crystals α-BBO (exp. 0.122 @ 532 nm) and $CaCO_3$ (exp. 0.172 @ 589 nm), and indeed it breaks through the birefringent limit of extant oxides (Table S5). The calculated linear optical properties (Figure 3c) show that the refractive index dispersion curves display strong anisotropy with $n_y > n_x > n_z$, indicating that $CeF_2(SO_4)$ is a biaxial negative crystal. The derived birefringence Δn is 0.36 @ 546 nm, in good agreement with measured birefringence. The shortest SHG phase-matching wavelength is 520 nm (Figure S7), confirming the phase-matching capability of $CeF_2(SO_4)$ under the experimental 1064 nm laser. To improve our understanding of the origin of the large birefringence of $CeF_2(SO_4)$, a real-space atom-cutting technique was adopted to evaluate the contribution of the constituent groups to the overall birefringence (Table S6). Clearly, the large birefringence of $CeF_2(SO_4)$ is mainly attributable to the optically anisotropic $[CeO_4F_4]$ units (0.33 @ 546 nm), while the contribution of the $[SO_4]$ unit is lower but still significant (0.10 @ 546 nm).

The IR absorption bands at 1200 and 900 cm^{-1} are assigned to $[SO_4]$ symmetric stretching (Figure S8), while other bands appearing around 616, 505, and 449 cm^{-1} are assigned to Ce-O/F asymmetric vibrations. The ultraviolet-visible-near-infrared (UV-Vis-NIR) diffuse reflectance spectrum (Figure S9) indicates that the band gap of $CeF_2(SO_4)$ is ca. 2.71 eV. Electronic band gap prediction by DFT resulted in an indirect band gap of 1.23 eV (Figure S10) for $CeF_2(SO_4)$, which is smaller than the experimental result, an outcome attributed to the derivative discontinuity of exchange-correlation energy. The partial densities of states of $CeF_2(SO_4)$ are shown in Figure S11. The electronic states of S and Ce overlap well with those of the O atoms from the VB to the CB, indicating strong covalent interactions in the S-O and Ce-O bonds. The top of the VB is dominated by O-2p nonbonding states, and in the bottom of the CB, the dominant orbital contributions come from Ce-4f orbitals mixed with a small amount of S-3p states. The band gap is therefore determined by Ce and O and the SHG response in $CeF_2(SO_4)$ mainly arises from the $[CeO_4F_4]$ units, because the NLO effect is determined by the virtual (electron and hole) excitations among the states near the forbidden band.

In summary, the first tetravalent rare-earth-metal fluorinated sulfate $CeF_2(SO_4)$ has been obtained by hydrothermal means through the combination of highly polarizable $[CeO_4F_4]$ polyhedra and sulfate. $CeF_2(SO_4)$ features the strongest SHG response (8 × KDP) among the reported sulfate-based NLO materials. Simultaneously, its birefringence (0.361 at 546 nm) exceeds those of the majority of oxides. Detailed theoretical calculations confirm that the remarkable linear and nonlinear optical properties mainly originate from the favorable alignment of the highly polarizable $[CeO_4F_4]$ units as well as $[SO_4]$ groups. This work sheds new light on the idea of introducing highly distorted fluorinated polyhedral such as $[CeO_4F_4]$ to improve the SHG response and birefringence of sulfate-based NLO materials, and will guide the discovery of other novel structure-driven NLO functional materials.

ASSOCIATED CONTENT

This Supporting Information is available free of charge via the Internet at http://pubs.acs.org.
Experimental details, crystallographic data, additional figures and tables of $CeF_2(SO_4)$ (PDF)
X-ray crystallographic file for CCDC number 2054273 (CIF)

AUTHOR INFORMATION

Corresponding Author

* E-mail: chizhang@tongji.edu.cn

Author Contributions

¶These authors contributed equally.

Notes

The authors declare no competing financial interest.

ACKNOWLEDGMENT

This research was financially supported by the National Natural Science Foundation of China (no. 51432006), the Ministry of Education of China for the Changjiang Innovation Research Team (no. IRT14R23), the Ministry of Education and the State Administration of Foreign Experts Affairs for the 111 Project (no. B13025), the Innovation Program of Shanghai Municipal Education Commission, and the National and Shanghai Postdoctoral Program for Innovative Talents (nos. BX201800216 and 2018192). M.G.H. thanks the Australian Research Council for support (DP170100411).

REFERENCES

(1) Cyranoski, D. Materials Science: China's Crystal Cache. *Nature* **2009**, *457*, 953-955.
(2) Becker, P. Borate Materials in Nonlinear Optics. *Adv. Mater.* **1998**, *10*, 979-992.
(3) Mutailipu, M.; Poeppelmeier, K. R.; Pan, S. L. Borates: A Rich Source for Optical Materials. *Chem. Rev.* **2021**, *121*, 1130-1202.
(4) Tran, T. T.; Young, J.; Rondinelli, J. M.; Halasyamani, P. S. Mixed-Metal Carbonate Fluorides as Deep-Ultraviolet Nonlinear Optical Materials. *J. Am. Chem. Soc.* **2017**, *139*, 1285-1295.
(5) Zou, G. H.; Jo, H.; Lim, S. J.; You, T. S.; Ok, K. M. Pb_2BO_3Cl: A Tailor-Made Polar Lead Borate Chloride with Very Strong Second Harmonic Generation. *Angew. Chem. Int. Ed.* **2016**, *55*, 12078-12082.
(6) Wu, C.; Lin, J.; Jiang, X. X.; Lin, Z. S.; Huang, Z. P.; Humphrey, M. G.; Halasyamani, P. S.; Zhang, C. $K_5(W_3O_9F_4)(IO_3)$: An Efficient Mid-Infrared Nonlinear Optical Compound with High Laser Damage Threshold, *Chem. Mater.* **2019**, *31*, 10100-10108.
(7) Nikogosyan, D. N. *Nonlinear Optical Crystals: A Complete Survey*, 1st ed.; Springer: New York, 2005; pp 5-173.
(8) Chen, C. T.; Wang, G. L.; Wang, X. Y.; Xu, Z. Y. Deep-UV Nonlinear Optical Crystal $KBe_2BO_3F_2$-Discovery, Growth, Optical Properties and Applications. *Appl. Phys. B: Lasers Opt.* **2009**, *97*, 9-25.

(9) Chen, C. T.; Wu, B. C.; Jiang, A. D.; You, G. M. A New-Type Ultraviolet SHG Crystal β-BaB_2O_4. *Sci. Sin. B* **1985**, *15*, 235-243.
(10) Chen, C. T.; Wu, Y. C.; Jiang, A. D.; Wu, B. C.; You, G. M.; Li, R. K.; Lin, S. J. New Nonlinear-Optical Crystal: LiB_3O_5. *J. Opt. Soc. Am. B* **1989**, *6*, 616-621.
(11) Okorogu, A. O.; Mirov, S. B.; Dergachev, A. Y.; Lee, W.; Crouthamel, D. I.; Vodopyanov, K. L.; Jenkins, N.; Badikov, V. V. Tunable Middle Infrared Downconversion in GaSe and $AgGaS_2$. *Opt. Commun.* **1998**, *155*, 307-312.
(12) Lei, B. H.; Yang, Z. H.; Yu, H. W.; Cao, C.; Li, Z.; Hu, C.; Poeppelmeier, K. R.; Pan, S. L. Module-Guided Design Scheme for Deep-Ultraviolet Nonlinear Optical Materials. *J. Am. Chem. Soc.* **2018**, *140*, 10726-10733.
(13) Tran, T. T.; Yu, H. W.; Rondinelli, J. M.; Poeppelmeier, K. R.; Halasyamani, P. S. Deep Ultraviolet Nonlinear Optical Materials. *Chem. Mater.* **2016**, *28*, 5238-5258.
(14) Halasyamani, P. S.; Rondinelli, J. M. The Must-have and Nice-to-have Experimental and Computational Requirements for Functional Frequency Doubling Deep-UV Crystals. *Nat. Commun.* **2018**, *9*, 2972.
(15) Wu, B. L.; Hu, C. L.; Mao, F. F.; Tang, R. L.; Mao, J. G. Highly Polarizable Hg^{2+} Induced a Strong Second Harmonic Generation Signal and Large Birefringence in $LiHgPO_4$. *J. Am. Chem. Soc.* **2019**, *141*, 10188-10192.
(16) Peng, G.; Ye, N.; Lin, Z. S.; Kang, L.; Pan, S. L.; Zhang, M.; Lin, C. S.; Long, X. F.; Luo, M.; Chen, Y.; Tang, Y. H.; Xu, F.; Yan, T. $NH_4Be_2BO_3F_2$ and γ-Be_2BO_3F: Overcoming the Layering Habit in $KBe_2BO_3F_2$ for the Next-Generation Deep-Ultraviolet Nonlinear Optical Materials. *Angew. Chem. Int. Ed.* **2018**, *57*, 8968-8972.
(17) Oseledchik, Y. S.; Prosvirnin, A. L.; Pisarevskiy, A. I.; Starshenko, V. V.; Osadchuk, V. V.; Belokrys, S. P.; Svitanko, N. V.; Korol, A. S.; Krikunov, S. A.; Selevich, A. F. New Nonlinear Optical Crystals: Strontium and Lead Tetraborates. *Opt. Mater*. **1995**, *4*, 669-674.
(18) Pan, F.; Shen, G. Q.; Wang, R. J.; Wang, X. Q.; Shen, D. Z. Growth, Characterization and Nonlinear Optical Properties of SrB_4O_7 Crystals. *J. Cryst. Growth* **2002**, *241*, 108-114.
(19) Pan, Y.; Guo, S. P.; Liu, B. W.; Xue, H. G.; Guo, G. C. Second-Order Nonlinear Optical Crystals with Mixed Anions. *Coord. Chem. Rev.* **2018**, *374*, 464-496.
(20) Liu, Y. S.; Jones, W. B.; Chernoch, J. P. High-Efficiency High-Power Coherent UV Generation at 266 nm in 90° Phase-Matched Deuterated KDP. *Appl. Phys. Lett.* **1976**, *29*, 32-34.
(21) Yu, P.; Wu, L. M.; Zhou, L. J.; Chen, L. Deep-Ultraviolet Nonlinear Optical Crystals: $Ba_3P_3O_{10}X$ (X = Cl, Br). *J. Am. Chem. Soc.* **2014**, *136*, 480-487.
(22) Li, L.; Wang, Y.; Lei, B.; H.; Han, S. J.; Yang, Z. H.; Poeppelmeier, K. R.; Pan, S. L. A New Deep-Ultraviolet Transparent Orthophosphate $LiCs_2PO_4$ with Large Second Harmonic Generation Response. *J. Am. Chem. Soc.* **2016**, *138*, 9101-9104.
(23) Chen, J.; Xiong, L.; Chen, L.; Wu, L. M. $Ba_2NaClP_2O_7$: Unprecedented Phase Matchability Induced by Symmetry Breaking and Its Unique Fresnoite-Type Structure. *J. Am. Chem. Soc.* **2018**, *140*, 14082-14086.
(24) Wu, C.; Yang, G.; Humphrey, M. G.; Zhang, C. Recent Advances in Ultraviolet and Deep-Ultraviolet Second-Order Nonlinear Optical Crystals. *Coord. Chem. Rev.* **2018**, *375*, 459-488.
(25) Wu, H. P.; Zhang, B. B.; Yu, H. W.; Hu, Z. G.; Wang, J. Y.; Wu, Y. C.; Halasyamani, P. S. Designing Silicates as Deep-UV Nonlinear Optical (NLO) Materials using Edge-Sharing Tetrahedra. *Angew. Chem. Int. Ed.* **2020**, *59*, 8922-8926.
(26) Li, Y. Q.; Liang, F.; Zhao, S. G.; Li, L. N.; Wu, Z. Y.; Ding, Q. R.; Liu, S.; Lin, Z. S.; Hong, M. C.; Luo, J. H. Two Non-π-Conjugated Deep-UV Nonlinear Optical Sulfates. *J. Am. Chem. Soc.* **2019**, *141*, 3833-3837.
(27) Netzsch, P.; Bariss, H.; Bayarjargal, L.; Höppe, H. A. $Tb(HSO_4)(SO_4)$ - A Green Emitting Hydrogensulfate Sulfate with Second Harmonic Generation Response. *Dalton Trans.* **2019**, *48*, 16377-16383.
(28) Yue, Z. H.; Lu, Z. T.; Xue, H. G.; Guo, S. P. $KBiCl_2SO_4$: The First Bismuth Chloride Sulfate Being Second-Order Nonlinear Optical Active. *Cryst. Growth Des.* **2019**, *19*, 3843-3850.
(29) Zhao, S. G.; Gong, P. F.; Luo, S. Y.; Bai, L.; Lin, Z. S.; Ji, C. M.; Chen, T. L.; Hong, M. C.; Luo, J. H. Deep-Ultraviolet Transparent Phosphates $RbBa_2(PO_3)_5$ and $Rb_2Ba_3(P_2O_7)_2$ Show Nonlinear Optical Activity from Condensation of $[PO_4]^{3-}$ Units. *J. Am. Chem. Soc.* **2014**, *136*, 8560-8563.
(30) Ok, K. M. Toward the Rational Design of Novel Noncentrosymmetric Materials: Factors Influencing the Framework Structures. *Acc. Chem. Res.* **2016**, *49*, 2774-2785.
(31) Dong, X. H.; Huang, L.; Hu, C. F.; Zeng, H. M. Lin, Z. E. Wang, X.; Ok, K. M.; Zou, G. H. $CsSbF_2SO_4$: An Excellent Ultraviolet Nonlinear Optical Sulfate with a $KTiOPO_4$ (KTP)-type Structure. *Angew. Chem. Int. Ed.* **2019**, *58*, 6528-6534.
(32) Yang, Y.; Qiu, Y.; Gong, P. F.; Kang, L.; Song, G. M.; Liu, X. M.; Sun, J. L.; Lin, Z. S. Lone-Pair Enhanced Birefringence in an Alkaline-Earth Metal Tin(II) Phosphate $BaSn_2(PO_4)_2$. *Chem. Eur. J.* **2019**, *25*, 5648-5651.
(33) Wu, C.; Jiang, X. X.; Wang, Z. J.; Lin, L.; Lin, Z. S.; Huang, Z. P. Humphrey, M. G.; Zhang, C. Giant Optical Anisotropy in the UV-transparent 2D Nonlinear Optical Material $Sc(IO_3)_2(NO_3)$, *Angew. Chem. Int. Ed.* **2021**, 60, 3464-3468.
(34) Zumsteg, F. C.; Bierlein, J. D.; Gier, T. E. $K_xRb_{1-x}TiOPO_4$: A New Nonlinear Optical Material. *J. Appl. Phys.* **1976**, *47*, 4980-4985.
(35) Yu, H. W.; Young, J.; Wu, H. P.; Zhang, W. G.; Rondinelli, J. M.; Halasyamani, P. S. Electronic, Crystal Chemistry, and Nonlinear Optical Property Relationships in the Dugganite $A_3B_3CD_2O_{14}$ Family. *J. Am. Chem. Soc.* **2016**, *138*, 4984-4989.
(36) Wu, C.; Jiang, X. X.; Lin, L.; Lin, Z. S.; Huang, Z. P.; Humphrey, M. G.; Zhang, C. $AGa_3F_6(SeO_3)_2$ (A = Rb, Cs): A New Type of Phase-Matchable Hexagonal Tungsten Oxide Material with Strong Second-Harmonic Generation Responses. *Chem. Mater.* **2020**, *32*, 6906-6915.
(37) Binnemans, K. Chapter 229 - Applications of Tetravalent Cerium Compounds. *In Handbook on the Physics and Chemistry of Rare Earths*; Gschneidner, K. A., Bunzli, J.-C. G., Pecharsky, V. K., Eds.; Elsevier, 2006; Vol. *36*; pp 281-392.
(38) Mao, F. F.; Hu, C. L.; Xu, X.; Yan, D.; Yang, B. P.; Mao, J. G. $Bi(IO_3)F_2$: The First Metal Iodate Fluoride with a Very Strong Second Harmonic Generation Effect. *Angew. Chem. Int. Ed.* **2017**, *56*, 2151-2155.
(39) Kohn, W. Nobel Lecture: Electronic Structure of Matter-Wave Functions and Density Functionals. *Rev. Mod. Phys.* **1999**, *71*, 1253-1266.
(40) Lin, J.; Lee, M. H.; Liu, Z. P.; Chen, C. T.; Pickard, C. J. Mechanism for Linear and Nonlinear Optical Effects in β-BaB_2O_4 Crystals. *Phys. Rev. B* **1999**, *60*, 13380-13389.
(41) He, R.; Lin, Z. S.; Lee, M. H.; Chen, C. T. Ab initio Studies on the Mechanism for Linear and Nonlinear Optical Effects in $YAl_3(BO_3)_4$. *J. Appl. Phys.* **2011**, *109*, 103510.

Table of Contents